NICST_MEMO_08_015

NICST Internal Memo

Date: April 7, 2008
From: J McIntire and C. Pan
To: Bruce Guenther, Jim Butler, Jack Xiong
Subject: VIIRS FU1 FP-13 Dynamic crosstalk, vertical slit test for SMWIR and LWIR

References:

[1] NICST_MEMO_07_027, VIIRS FU1 Dynamic Crosstalk in the VisNIR bands from STR-351, C. Pan and N. Che.

1. Introduction

VIIRS FU1 FP-13 ambient phase II includes a comprehensive crosstalk test. This work is concerned with the dynamic crosstalk tests for the SMWIR and LWIR bands in FP-13 which use the vertical slit (reticle 12 with an overlay mask). BandPass Filters (BPF) were utilized to insure that each UAID has a unique sender band and to minimize optical contamination. The illumination sources used here were the TMC BB and SIS; the TMC shutter was also employed. The low gain mode used the Default DPP & M16B APID band substitution tables and the auto gain mode used the M16A DPP & APID tables / Default DPP & M16B APID tables; the band substitution tables are given in Table 1. Out Of Band (OOB) response, as well as optical crosstalk, are obtained by examining this test data.

Tables 2 and 3 list the following test configuration information for the SMWIR and LWIR bands, respectively: UAID, filter utilized, source type (TMC BB or SIS), source irradiance, collects used, and gain mode. The focal plane sample timing is shown in Figure 1.

2. Data processing

Each UAID listed has two or three collects, listed in Tables 2 and 3. Every one of these collects contains 256 scans (in diagnostic mode). For each scan, only the samples near the position of direct illumination for each band were processed (samples 970-1069 for M bands and samples 1940-2139 for I bands). The scans followed a pattern of two scans with the shutter open then two scans with the shutter closed. The dn (for each band, HAM side, detector, subsample, sample, and shutter) are averaged over scans; then, the shutter closed scans were used as a background subtraction. Next, a baseline average was computed from the scan averaged, background subtracted samples that were more than 30 samples away from the position of direct illumination, but still within the samples under consideration. This baseline was then subtracted from the scan averaged, background subtracted dn.

For the special case of auto gain (ag), when the sender band is in auto low gain for a few samples but the remaining samples are in high gain for a given scan, the normal background subtraction procedure is not appropriate because the background is in high gain. One needs to convert the low gain samples from low to high gain; this is accomplished by introducing an extra gain factor as shown by

$$dn_{ag} = DN_{ag} \frac{g_{hg}}{g_{\mathrm{lg}}}. \tag{1}$$

Here g_{hg} and g_{lg} are the radiometric gains of the detector in question for high and low gain states respectively.

We must also consider the problem imposed by band substitution; if a sender band has been excluded from the reported data, then the shutter order cannot be determined. As can be seen from the band substitution tables listed in Table 1, this problem exists for sender bands M12, M13, M14, M15, and M16A. Fortunately, one can see a clear difference between the shutter open and closed scans in the OOB response of selected receiver bands; those corresponding bands are I4, I4, M15, I5, and M16B, respectively. The OOB response from M13 auto high gain to I4 and from M14 to M15 is small, but the peak is still easily discernable. Using this approach the shutter order was reconstructed for the collects where the sender band was not recorded.

In order to get a quantitative idea of the crosstalk observed in these tests, we introduce two coefficients, following from [1]. To calculate these coefficients, we first determine the maximum dn and radiance as a function of frames for each band, HAM side, detector, and subsample. Then, the first coefficient is the ratio of the maximum receiver dn to the maximum sender dn averaged over detectors and subsamples, or

$$XF_{dn} = \frac{dn_{REC}^{b,h,d,s}(i)}{\left\langle dn_{SND}^{b,h,d,s}(j) \right\rangle_d}. \tag{2}$$

Note that dn is a function of band (b), HAM side (h), detector (d), and subsample (s). The i's and j's indicate the gain state of the quantity in question. The second coefficient is the ratio of the maximum receiver radiance to the maximum sender radiance averaged over detectors and subsamples, or

$$XF_{L} = \frac{L_{REC}^{b,h,d,s}(i)}{\left\langle L_{SND}^{b,h,d,s}(j) \right\rangle_d}. \tag{3}$$

Note that the radiance is the ratio of dn to gain. All the SMWIR and LWIR bands except M13 are single-gain, so consideration of different gain states is only necessary in cases involving band M13.

These coefficients are collected into an OOB response table for both the SMWIR and LWIR bands. A portion of this table is shown in Table 4; the full tables are available upon request.

3. Analysis - LWIR

Besides the expected optical response due to spectral overlap between bands M16A, M16B, and I5, the main feature in the LWIR is OOB response. In Figure 2, the OOB response from sender band M15 is shown; here, there is a large OOB response in band I5 and smaller OOB peaks in bands M16A and M16B. In addition, the sample timing for M16A relative to the other bands is offset by 5 frames.

In Figure 3, there is a large OOB response from sender band I5 to M15 in addition to the response due to spectral overlap observed in bands M16A and M16B. Optical crosstalk is also observed on the right side of the I4 peaks; small crosstalk peaks are observed at the positions of M16A even, M16B odd, and M16B even for subsample 1 (SS1). The shape of the response in subsample 2 (SS2) is inverted from that of SS1.

Figure 4 shows the instrument response when the BPF M14 is used. There are small OOB response peaks for bands M15, M16A, M16B, and I5. Also, optical crosstalk in band M14 is evident at position M15 odd and M16B even for odd detectors and at positions M15 even and M16B even for even detectors. This odd – even detector difference is the result of the staggering of the detectors.

Optical response due to spectral overlap is observed in bands M16B and I5 Figure 5, where the M16A BPF was used. Additionally, there is a small OOB response in bands M15. Similar results were observed when the BPF M16B was used.

There is a thermal leak in the TEB bands when the shutter is closed. This effect is shown in Figure 6 for BPF M14 (the top graph is shutter open and the bottom graph is shutter closed). For shutter closed scans, there is a peak at the position where the light would illuminate band M14. This is light that is re-radiated from the shutter. This effect is consistent over scans and BPFs for all the TEB bands, but is most prominent in the LWIR bands and M13 in low gain. Using the shutter closed scans as a background subtraction, the coefficients are overestimated by up to 5 %. In addition, this thermal effect sometimes produces a negative peak in the raw data, as seen in Figure 7 (the top graph is shutter open and the bottom graph is shutter closed).

4. Analysis – SMWIR

Besides the expected optical response due to spectral overlap between bands M12 and I4 and between bands M10 and I3, the main feature in the SMWIR is OOB response. Figures 8 and 9 show the OOB response in bands M12, M13, and I4 using the BPF M8. In addition, these figures display optical crosstalk on the left hand side of the M8 peak corresponding to the position M11 even for both odd and even M8 detectors.

In Figure 10, there is some small OOB response in bands M13, M12, and I4 using the BPF M10; there is also some optical crosstalk from M11 odd to both odd and even detectors in band M10. The expected optical response due to spectral overlap is also observed in band I3. Similar results were observed when the BPF I3 was used.

A small amount of OOB response in band M13 is evident in Figure 11, where the BPF M9 was used. Also, optical crosstalk is observed from band M8 even to both odd and even M9 detectors.

The Figure 12 shows a small OOB response in band M13 for the M12 BPF. In addition, band I4 sends optical crosstalk to band M12 and band I3 sends a small amount of electrical crosstalk to band I4. The expected optical response due to spectral overlap is also observed in band I4. Similar effects are seen when the I4 BPF is used, as shown by Figure 13.

Figures 14 – 16 show dynamic crosstalk results using the BPF M13 for auto high gain, auto low gain, and fixed low gain, respectively. In all three, there is OOB response in bands M12 and I4; this response is small in auto low gain and higher in auto low and fixed low gains. Additionally, optical crosstalk is observed in auto high and auto low gains from band M12 even and I4 to M13 even and from M12 odd and I4 to M13 odd.

Data for the BPF M11 was not collected; as a result, no analysis or conclusions regarding dynamic crosstalk from this band can be made.

Summary

- No evidence of dynamic crosstalk observed.
- Major OOB response evident from M15 to I5, from I5 to M15, and from M13 (auto low and fixed low gains) to M12 and I4.
- Optical crosstalk observed in M8 and M10 from M11, in M9 from M8, in M12 from I4, in M13 (auto high and auto low gains) from M12 and I4, in I5 from M16A and M16B, and in M14 from M15 and M16B.
- Some odd – even dependence evident in optical crosstalk.
- Thermal leak observed in TEB bands.

Acknowledgement

The sensor test Data used in this document was provided by the SBRS testing team. Approaches for data acquisition and data reductions, as well as data extraction tools were also provided by the SBRS. We would like to thank the SBRS team for their support.

Table 1: FU1 FP-13 band substitution table

Default DPP & M16B APID	M16A DPP & APID
M6	M16A
M12	DNBHGA
M13	DNBHGB
M14	DNBMGS
M15	DNBLGS

Table 2: FU1 FP-13 dynamic crosstalk, vertical slit test configurations for SMWIR bands

UA ID	BPF	Source	Illumination Level (fl) / Temperature (C)	Collects	Gain Settings
3102099	M8	TMC SIS	7800	6, 7	Auto
3102103	M10	TMC SIS	4800	6, 7	Auto
3102105	I3	TMC SIS	4300	8, 9	Auto
3102117	M9	TMC SIS	4200	6, 7	Auto
3102121	M12	TMC BB	115	7, 8	Auto
3102149	I4	TMC BB	97	5, 6	Auto
3102162	M13	TMC BB	95	9, 10	Auto
3102166	M13	TMC BB	425	8, 9, 10	Auto / Low
3102167	M13	TMC BB	598	8, 9, 10	Auto / Low

Table 3: FU1 FP-13 dynamic crosstalk, vertical slit test configurations for LWIR bands

UA ID	BPF	Source	Temperature (C)	Collects	Gain Settings
3102125	M14	TMC BB	135	5, 6	Auto
3102154	M16A	TMC BB	187	4, 5	Auto
3102156	M16B	TMC BB	196	5, 6	Auto
3102158	I5	TMC BB	145	5, 6	Auto
3102160	M15	TMC BB	175	7, 8	Auto

Table 4: FU1 FP-13 dynamic, vertical slit test OOB response in radiance space (using Eq. 3) from M15, HAM side A

UAID	Detector	HAM	M14	M15	M16A	M16B	I5 SS1	I5 SS2
3102160	1	A	0.0274875	0.9904112	0.1641156	0.1603167	1.1351124	0.9677774
3102160	2	A	0.0278783	0.9997469	0.1600341	0.1575086	1.1772591	0.9875711
3102160	3	A	0.0284937	0.9965684	0.1587539	0.1564942	1.1236368	0.9597769
3102160	4	A	0.0285506	1.0059305	0.1599277	0.1502737	1.1684666	0.9806407
3102160	5	A	0.0290689	0.996186	0.1526462	0.1554206	1.1147449	0.9533716
3102160	6	A	0.0292094	1.0035452	0.1529268	0.1525606	1.159395	0.9735374
3102160	7	A	0.0297232	0.9957592	0.1535708	0.1539606	1.1110435	0.9528289
3102160	8	A	0.0297295	1.0063295	0.1499615	0.1559199	1.1552738	0.9712675
3102160	9	A	0.0296884	1.0009025	0.1546564	0.1536277	1.1078218	0.9470882
3102160	10	A	0.0295131	1.006391	0.1558468	0.1512019	1.1516989	0.9655931
3102160	11	A	0.0300933	0.9968019	0.1541249	0.1547981	1.1036378	0.9449431
3102160	12	A	0.0298233	1.0055501	0.1555642	0.1512191	1.1530451	0.9685056
3102160	13	A	0.0301011	0.9974459	0.1571831	0.1540565	1.1045434	0.9493957
3102160	14	A	0.0302362	1.003378	0.1562115	0.1532229	1.1491711	0.9667981
3102160	15	A	0.0311466	0.9959762	0.1546652	0.1593777	1.1022612	0.9513624
3102160	16	A	0.0315888	0.999077	0.1549724	0.1572753	1.148738	0.9681074
3102160	17	A	-999	-999	-999	-999	1.099722	0.9518648
3102160	18	A	-999	-999	-999	-999	1.1499661	0.972899
3102160	19	A	-999	-999	-999	-999	1.1033881	0.9555492
3102160	20	A	-999	-999	-999	-999	1.1558858	0.9784983
3102160	21	A	-999	-999	-999	-999	1.1080872	0.9612804
3102160	22	A	-999	-999	-999	-999	1.1534936	0.9773526
3102160	23	A	-999	-999	-999	-999	1.1057565	0.9603662
3102160	24	A	-999	-999	-999	-999	1.1556219	0.9858581
3102160	25	A	-999	-999	-999	-999	1.1131705	0.9684084
3102160	26	A	-999	-999	-999	-999	1.1565675	0.9870576
3102160	27	A	-999	-999	-999	-999	1.1171805	0.974036
3102160	28	A	-999	-999	-999	-999	1.1643679	0.9939936
3102160	29	A	-999	-999	-999	-999	1.1144933	0.9707429
3102160	30	A	-999	-999	-999	-999	1.1622312	0.9919721
3102160	31	A	-999	-999	-999	-999	1.1191527	0.9787344
3102160	32	A	-999	-999	-999	-999	1.1665248	0.9945725

Figure 1: Focal plane layouts and sample timing (M16_1 is M16A and M16_2 is M16B in the text)

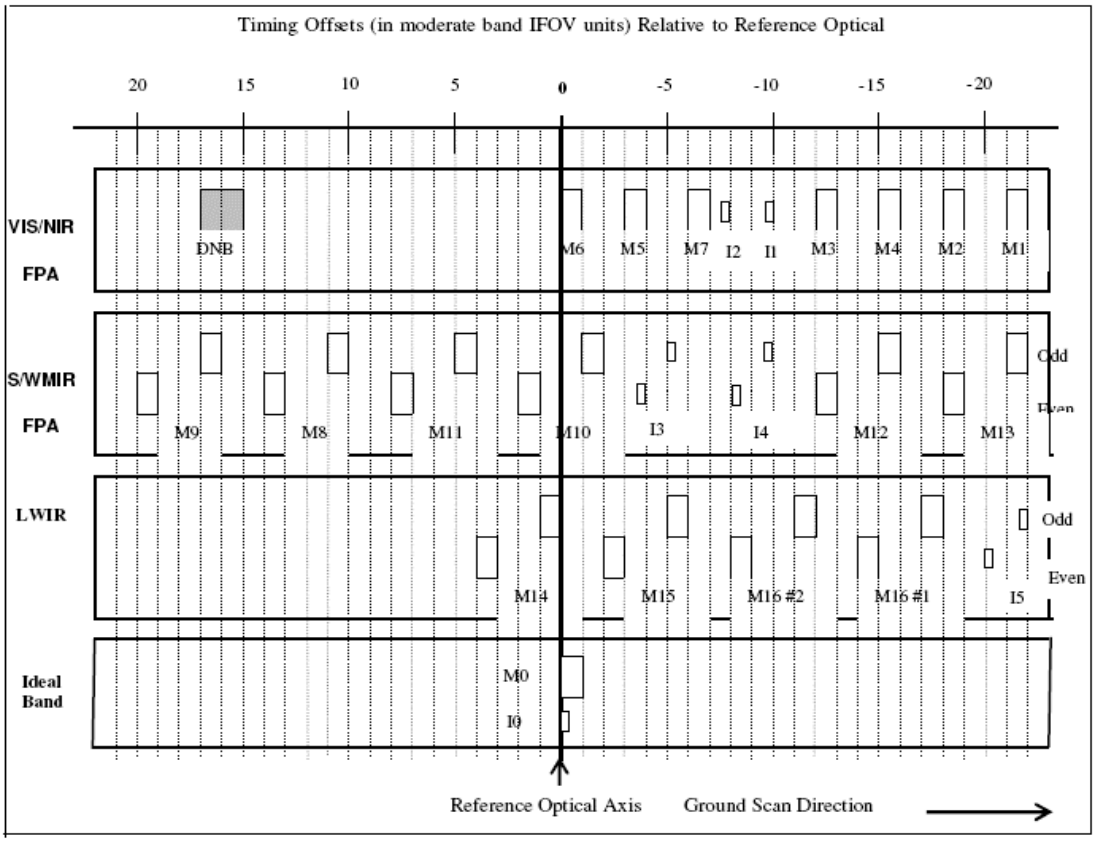

Figure 2: De-registered graphs of LWIR bands for BPF M15, detector 2

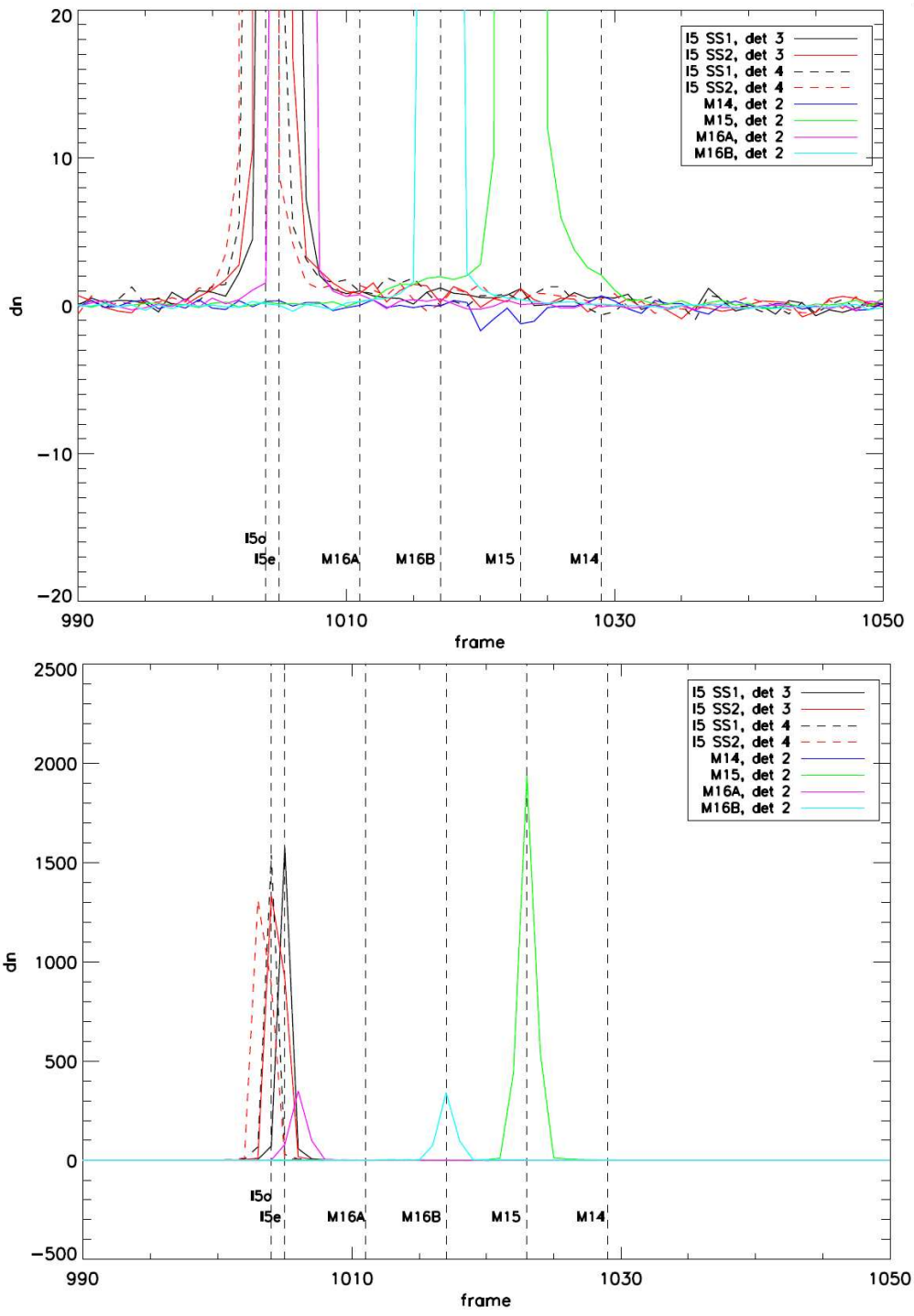

Figure 3: De-registered graphs of LWIR bands for BPF I5, detectors 19 and 20

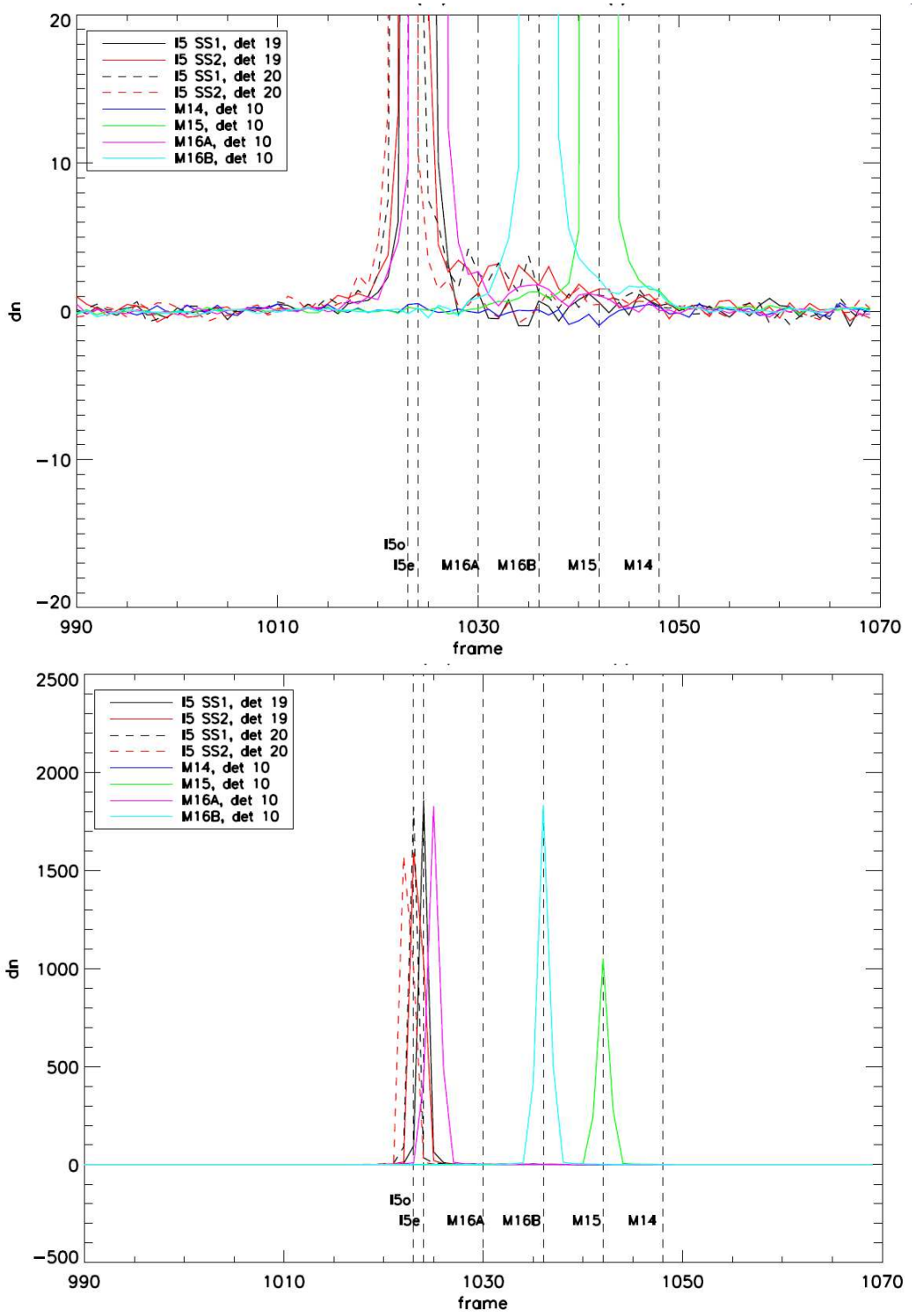

Figure 4: De-registered graphs of LWIR bands for BPF M14, detectors 5 and 6

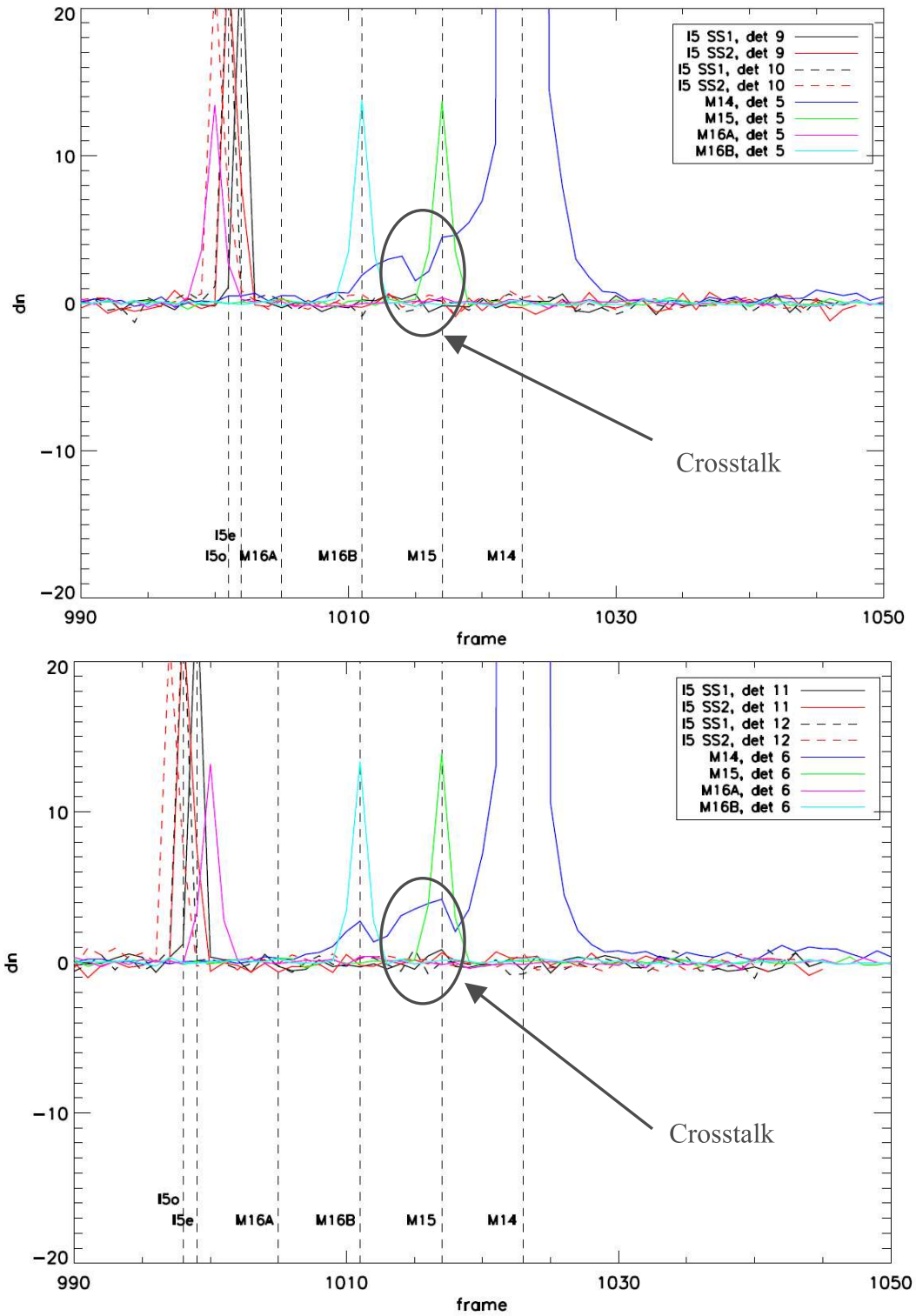

Figure 5: De-registered graphs of LWIR bands for BPF M16A, detector 9

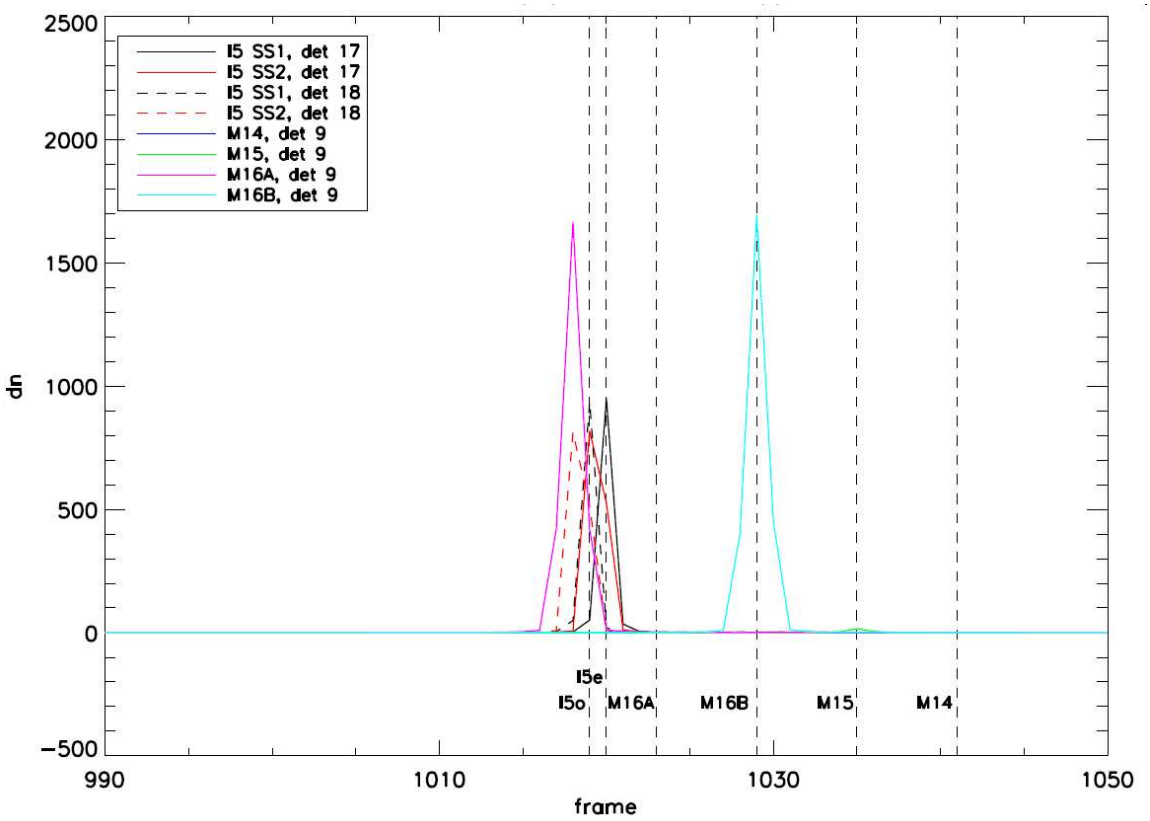

Figure 6: Thermal leak for band M14 using BPF M14

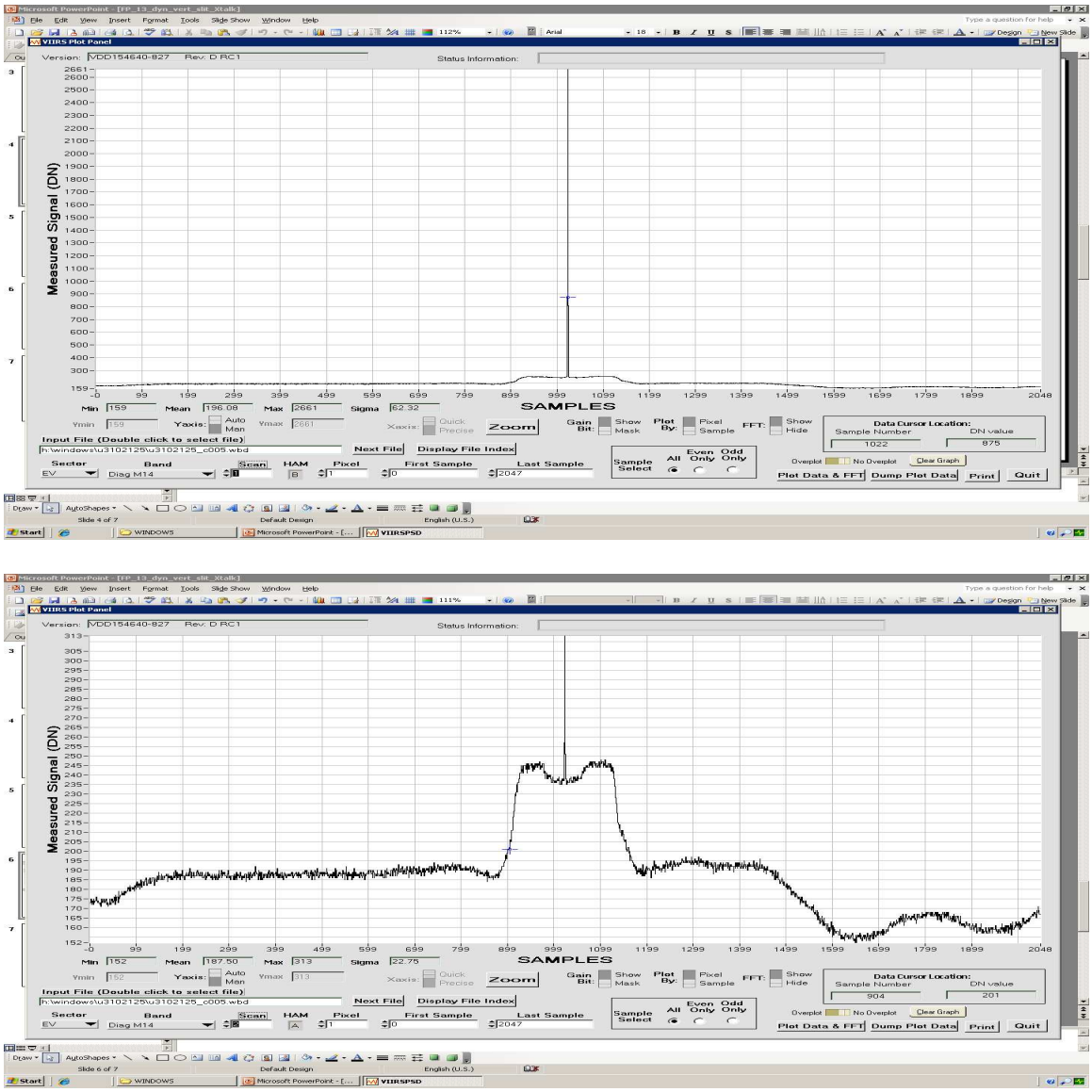

Figure 7: Thermal leak for band M16B using BPF M14

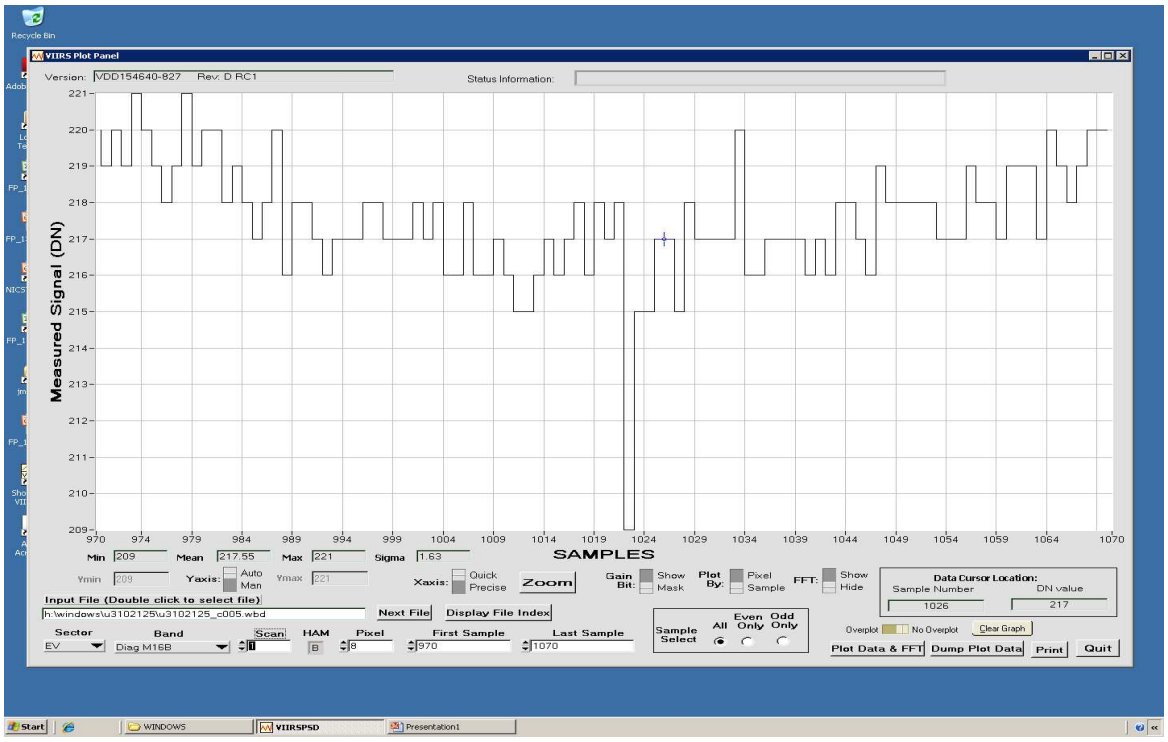

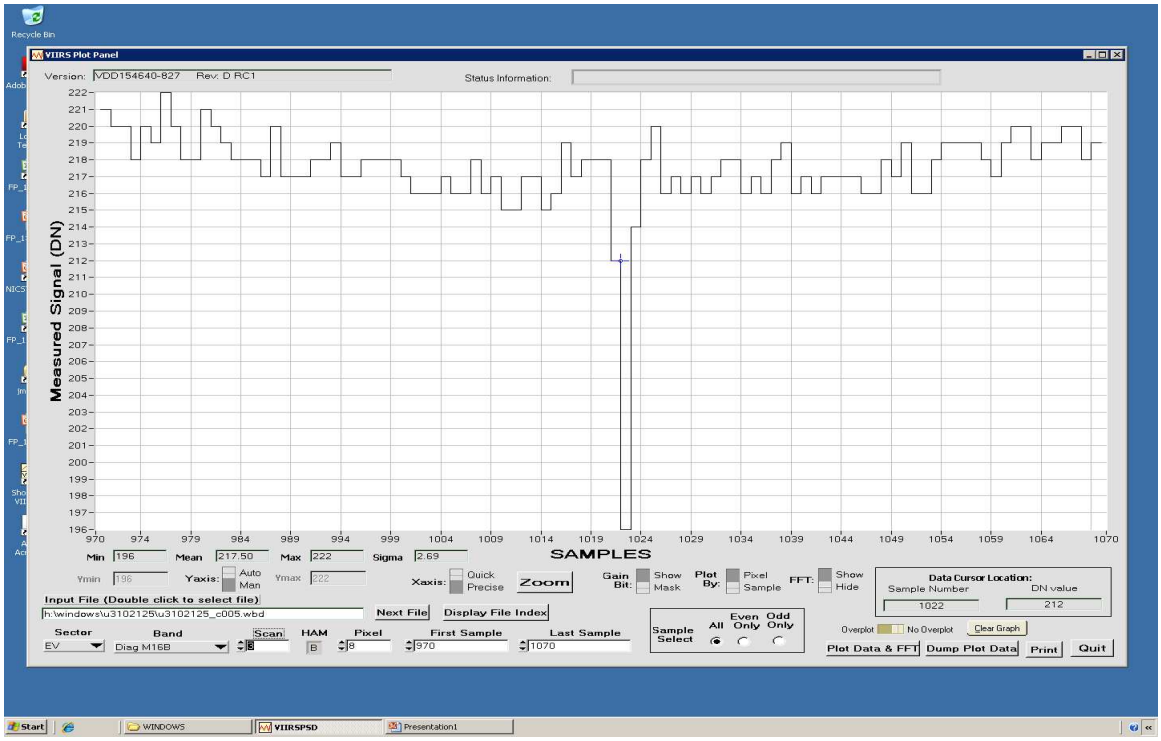

Figure 8: De-registered graphs of SMWIR bands for BPF M8, detector 8

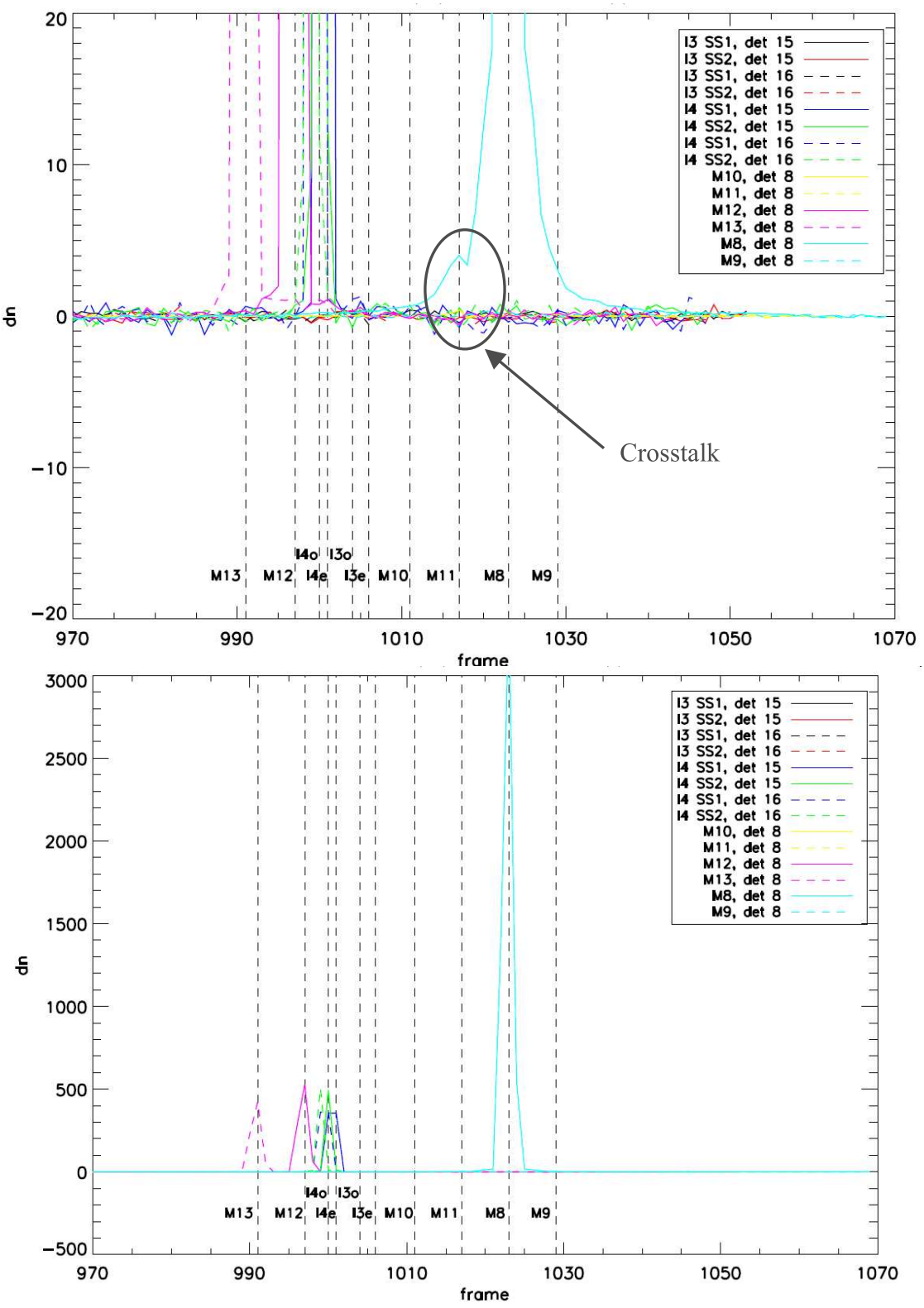

Figure 9: De-registered graphs of SMWIR bands for BPF M8, detector 9

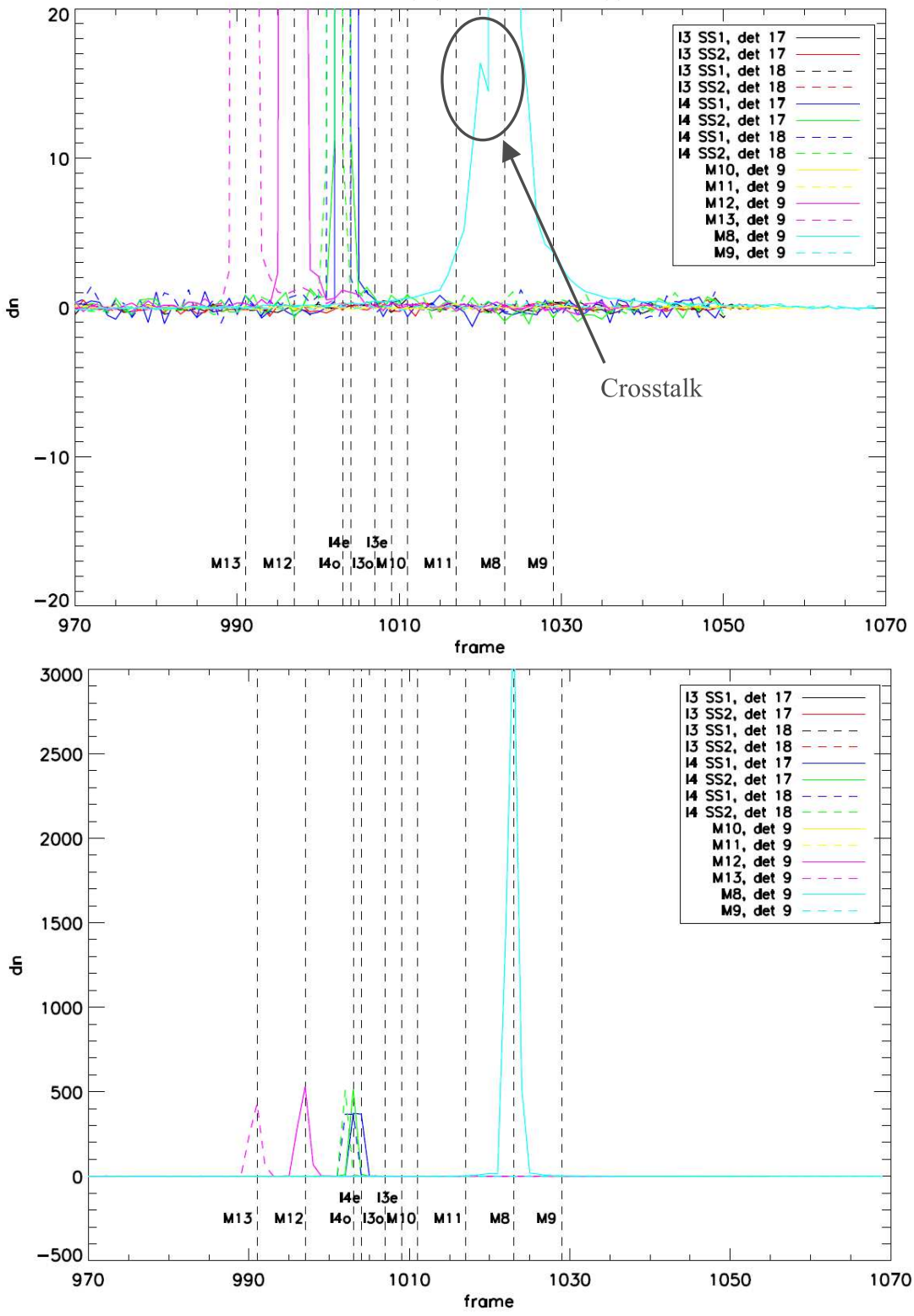

Figure 10: De-registered graphs of SMWIR bands for BPF M10, detectors 3 and 4

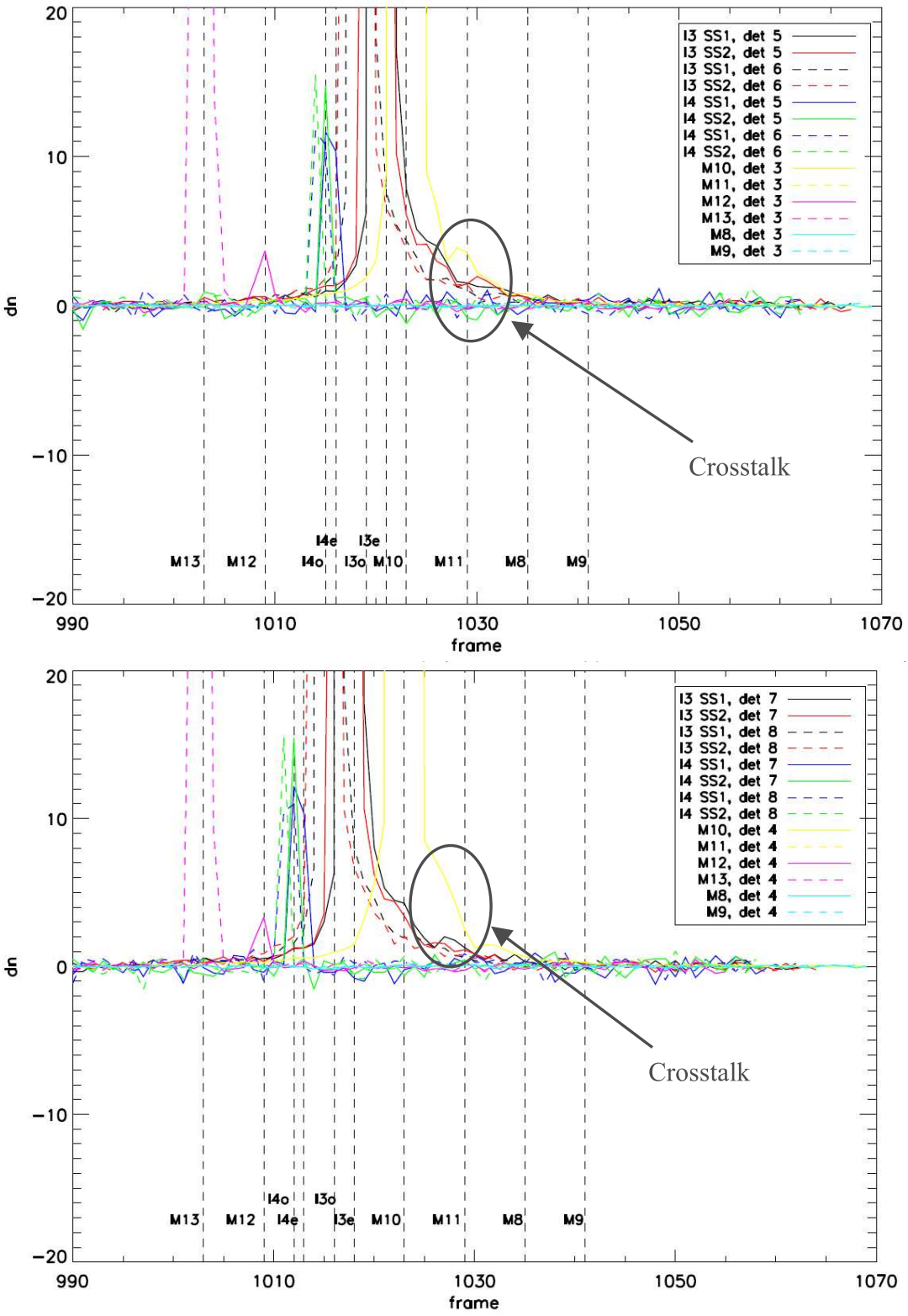

Figure 11: De-registered graphs of SMWIR bands for BPF M9, detectors 8 and 9

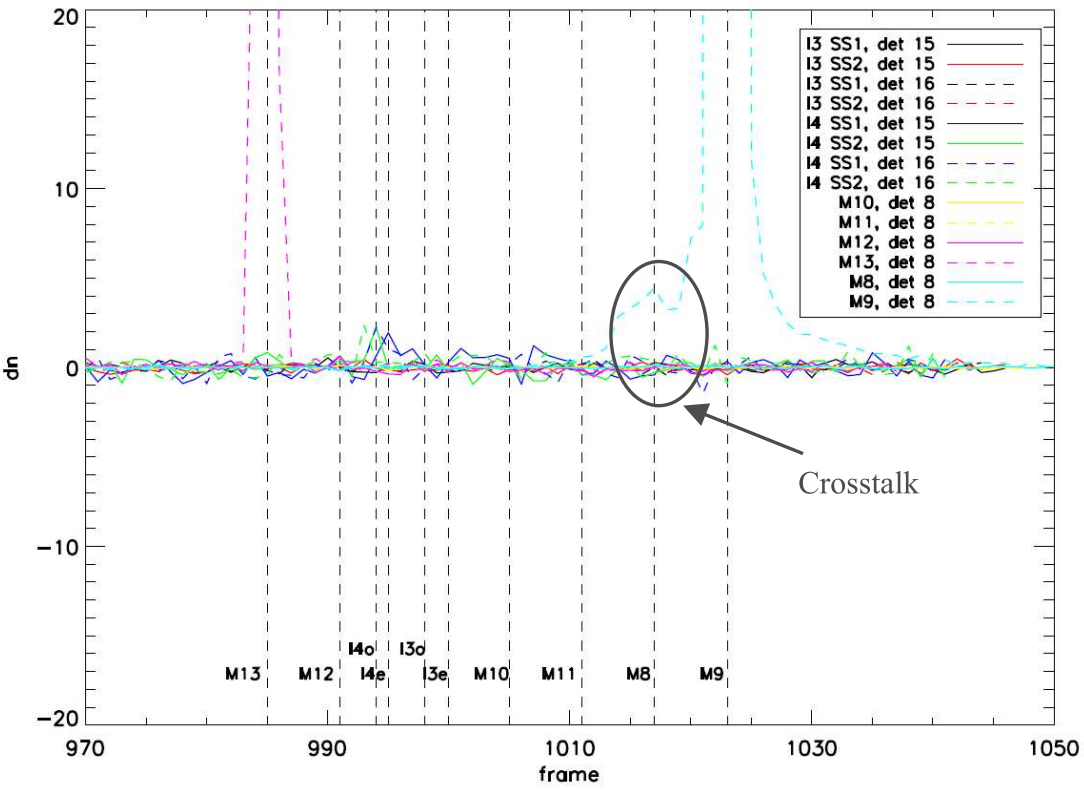

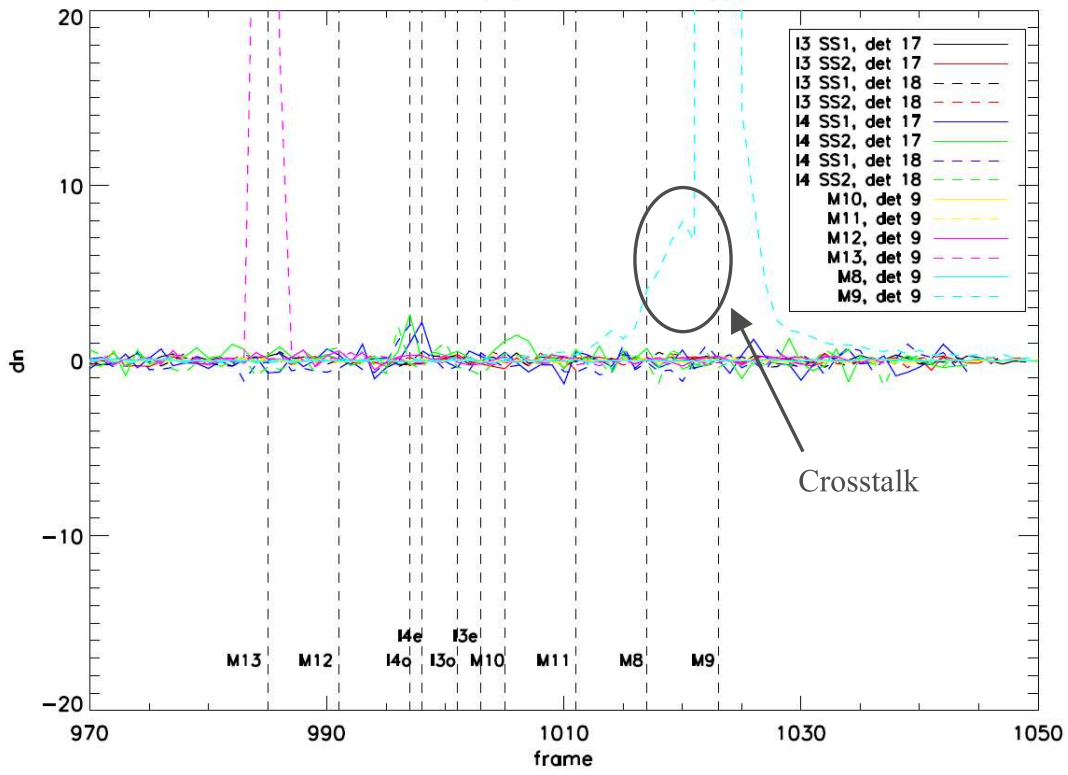

Figure 12: De-registered graphs of SMWIR bands for BPF M12, detectors 3 and 4

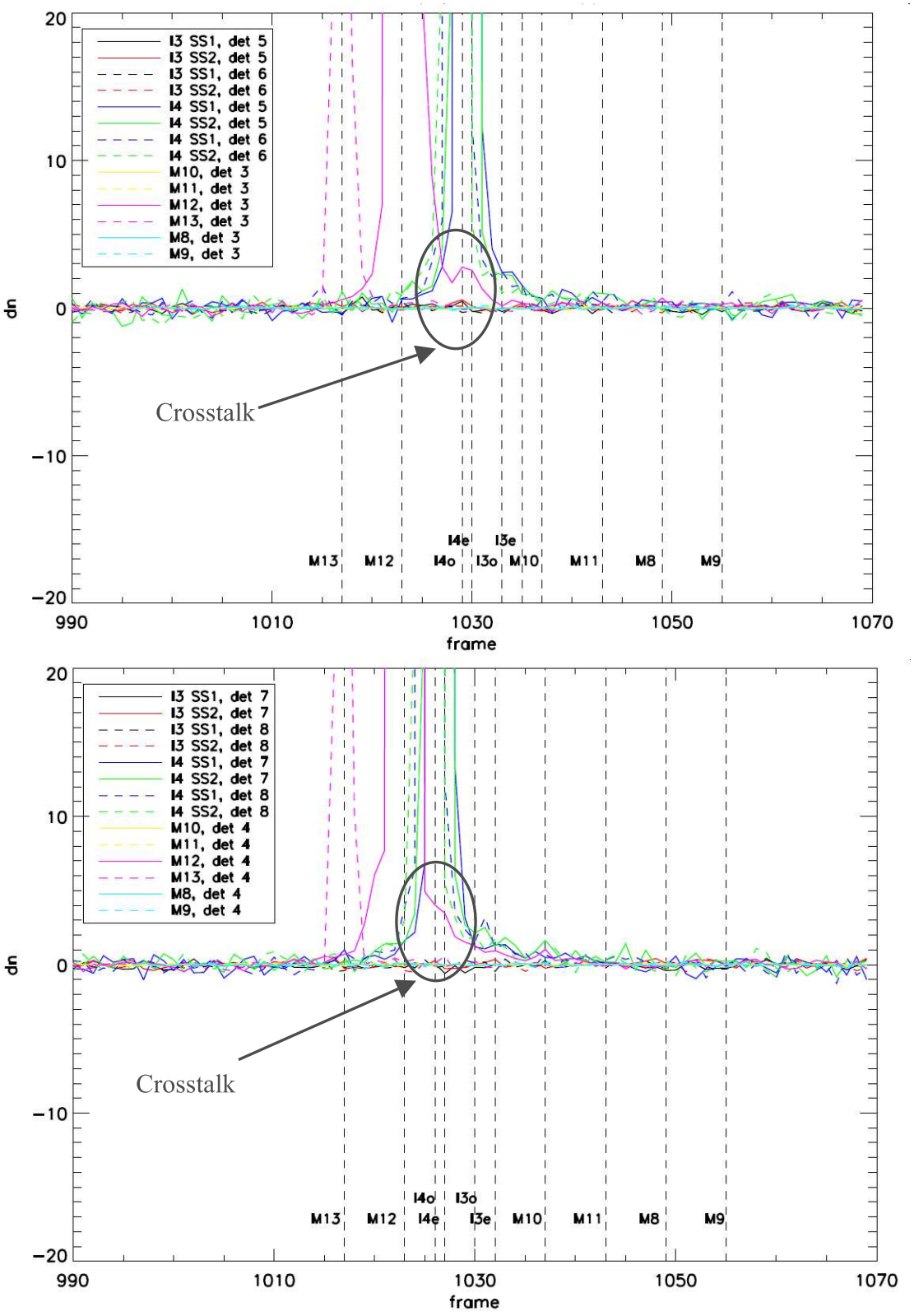

Figure 13: De-registered graphs of SMWIR bands for BPF I4, detector 15

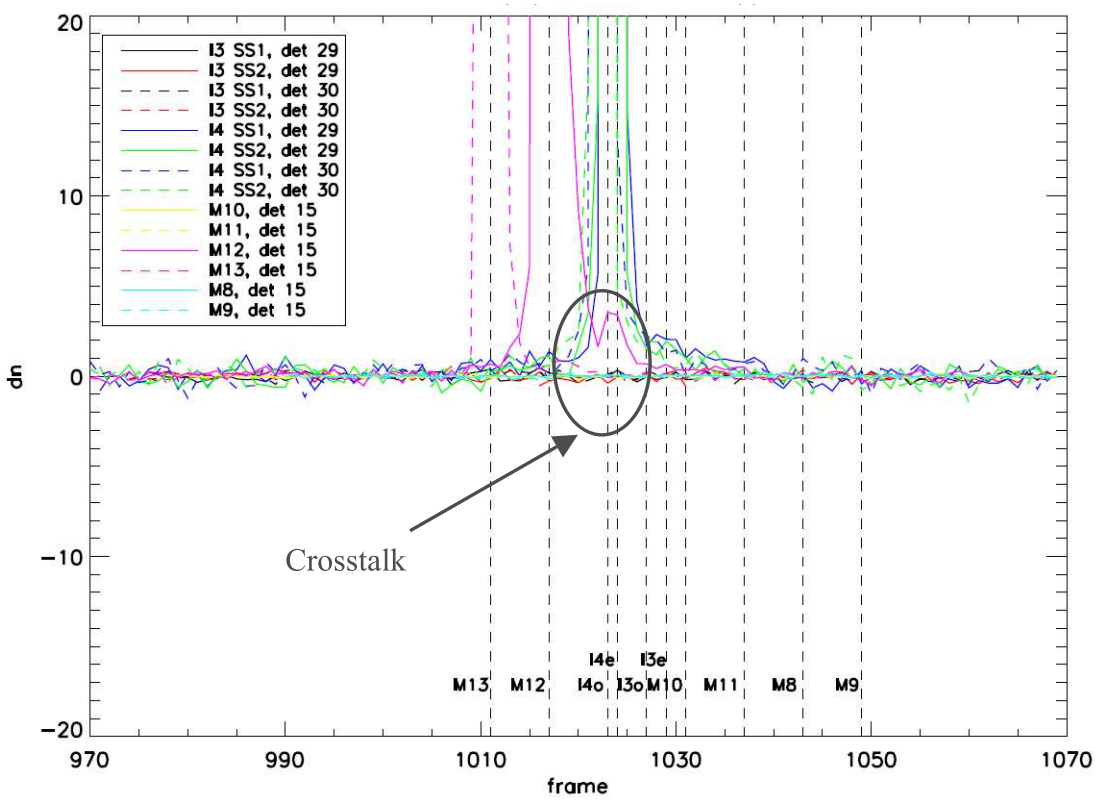

Figure 14: De-registered graphs of SMWIR bands for BPF M13 auto high gain, detectors 7 and 8

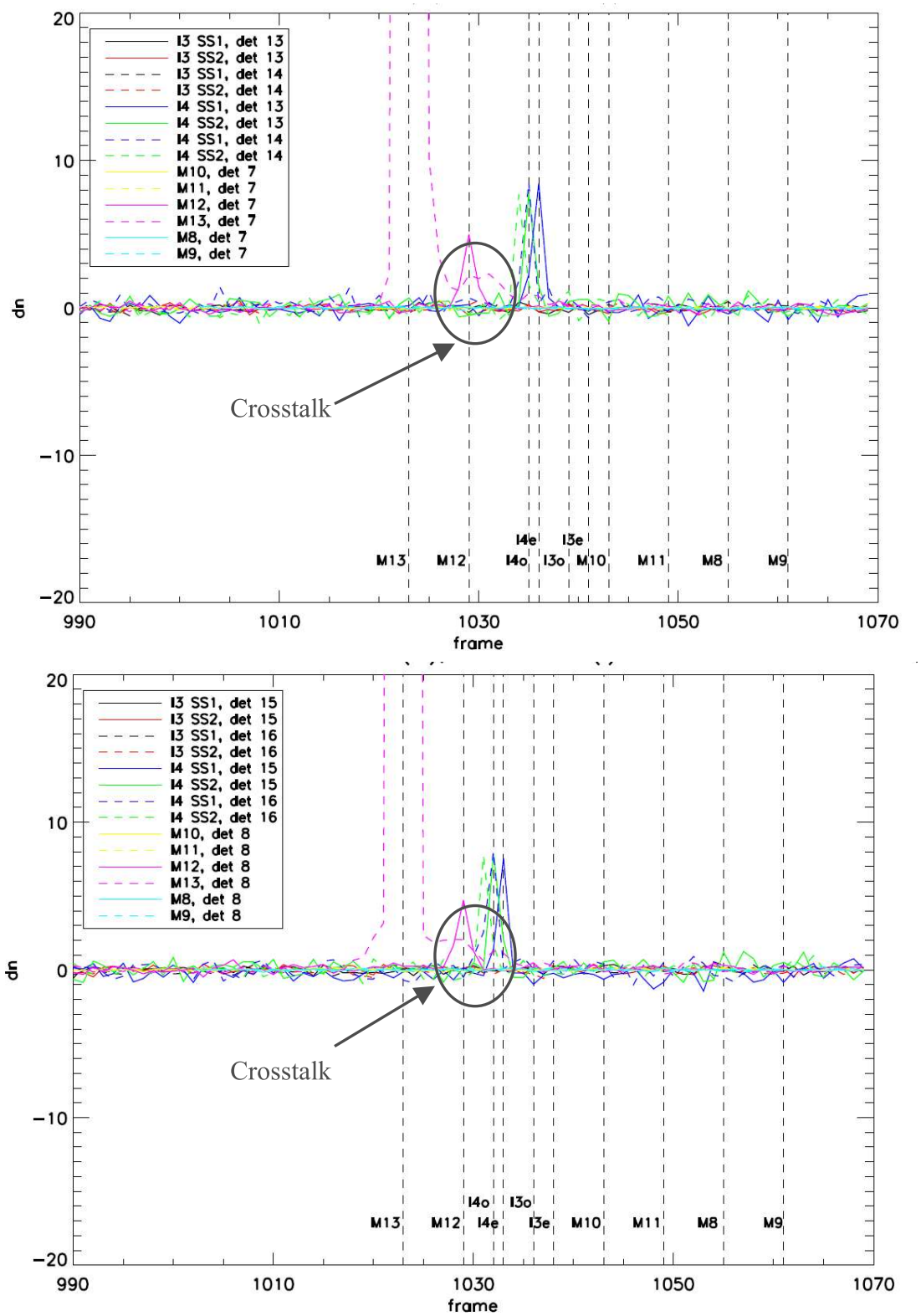

Figure 15: De-registered graphs of SMWIR bands for BPF M13 auto low gain, detector 8

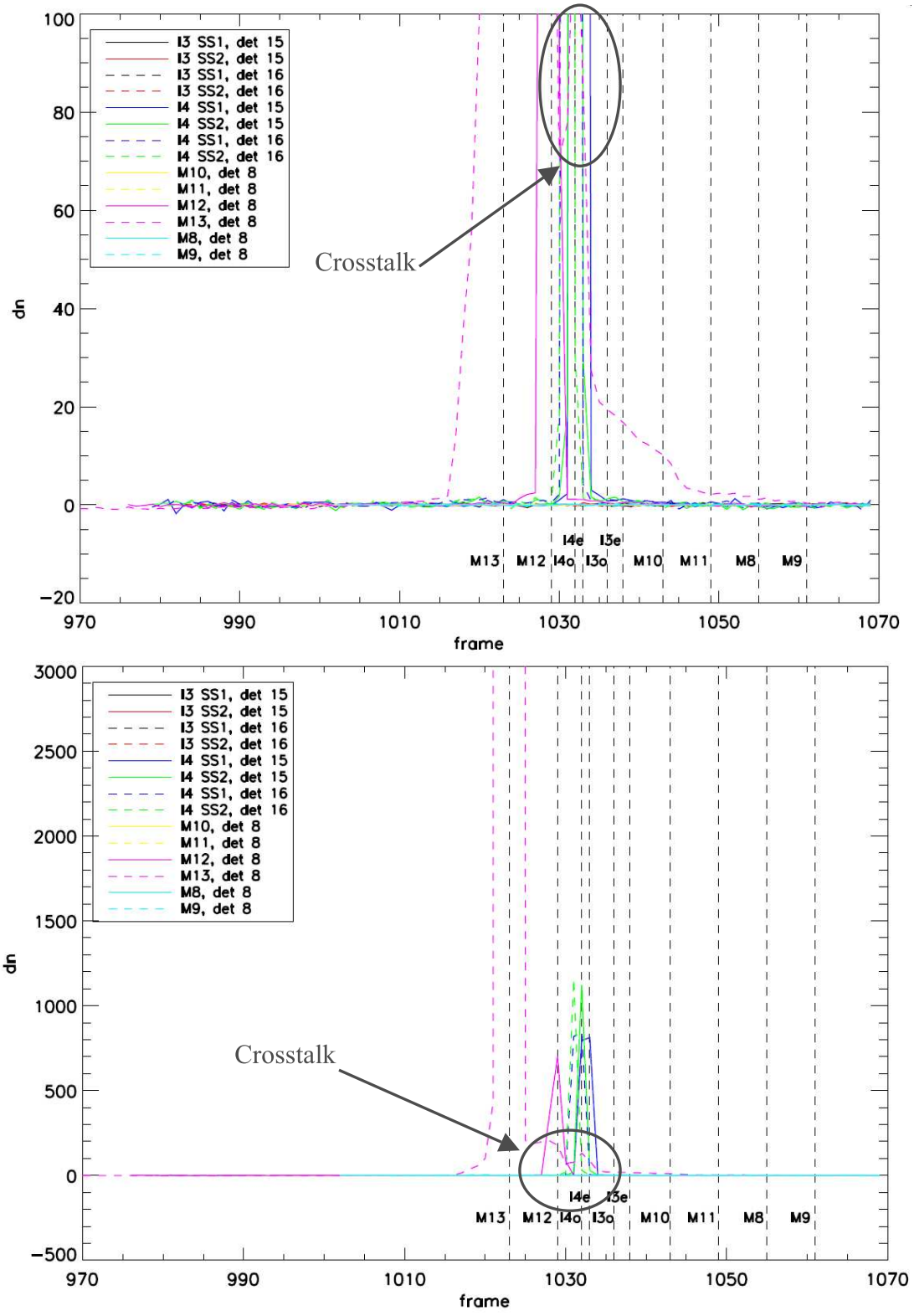

Figure 16: De-registered graphs of SMWIR bands for BPF M13 fixed low gain, detector 8